Supporting Information

Performance analysis of photo-liquefiable azobenzene derivatives for improving the responsive ability of their functional devices

Jing Hu[ac], *Mingming Yu*[b] and *Haifeng Yu**[c]

a. School of Mechanical Engineering, Shenyang University, Shenyang, 110044, Liaoning, China
b. College of Chemistry and Molecular Engineering, Zhengzhou University, Zhengzhou, 450001, China
c. School of Materials Science and Engineering, Key Laboratory of Polymer Chemistry and Physics of Ministry of Education, Peking University, Beijing, 100871, China.
*Email: yuhaifeng@pku.edu.cn

Content

1. Supplementary Figures

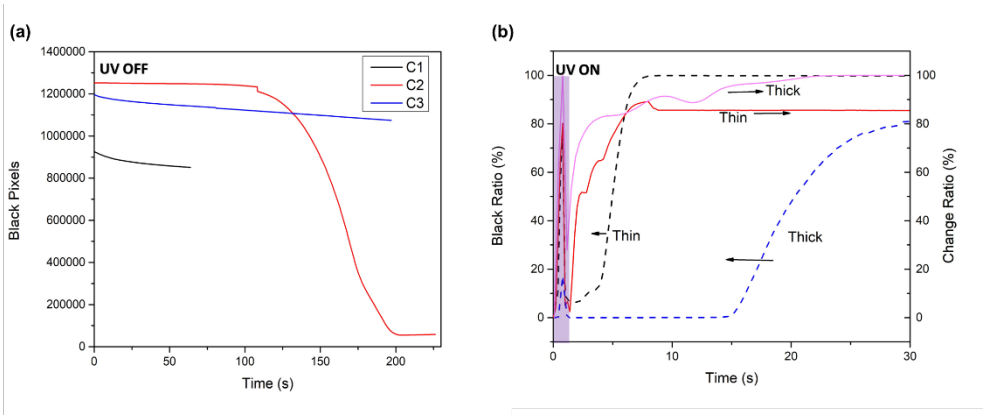

Fig. S1 (a) Black Area Pixel Statistical (BAPS) method was used to analyze the phase transition recovery phase, and the starting time was aligned with the moment when UV light was turned off; (b) Comprehensive analysis results of the two thickness of compound C2 samples by BAPS and RFDA methods (Thick sample ~5 μm, Thin sample ~3 μm).

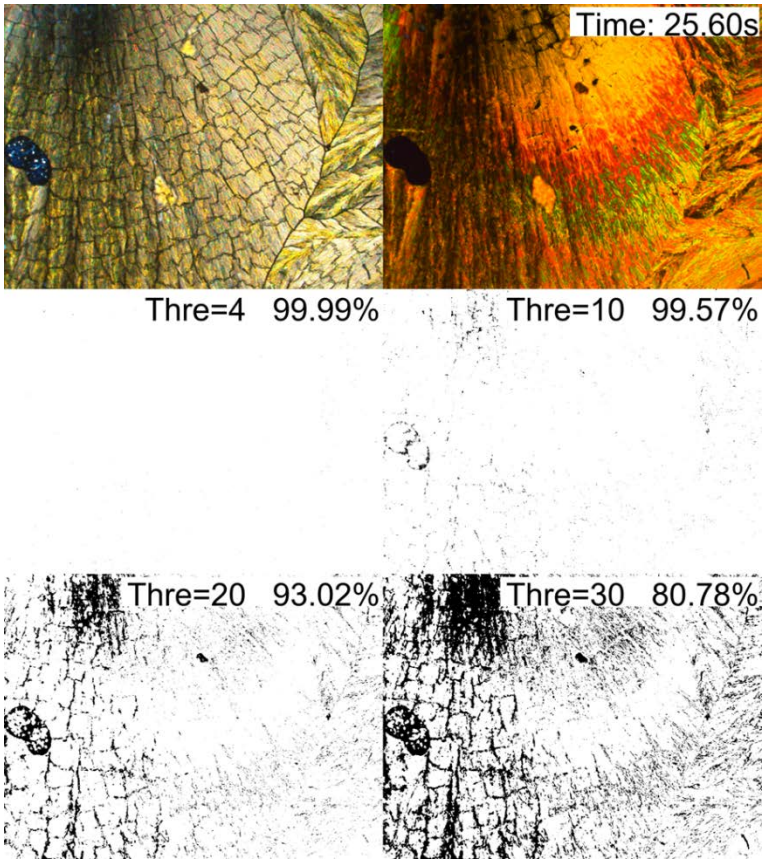

Fig. S2 Demonstration of RFDA method. (a) Photos of the original condition of C1 sample; (b) Screenshot of the status when UV illumination time was 25.6 s; (c-f) Compare figure a and b pixel by pixel to calculate the difference under different thresholds.

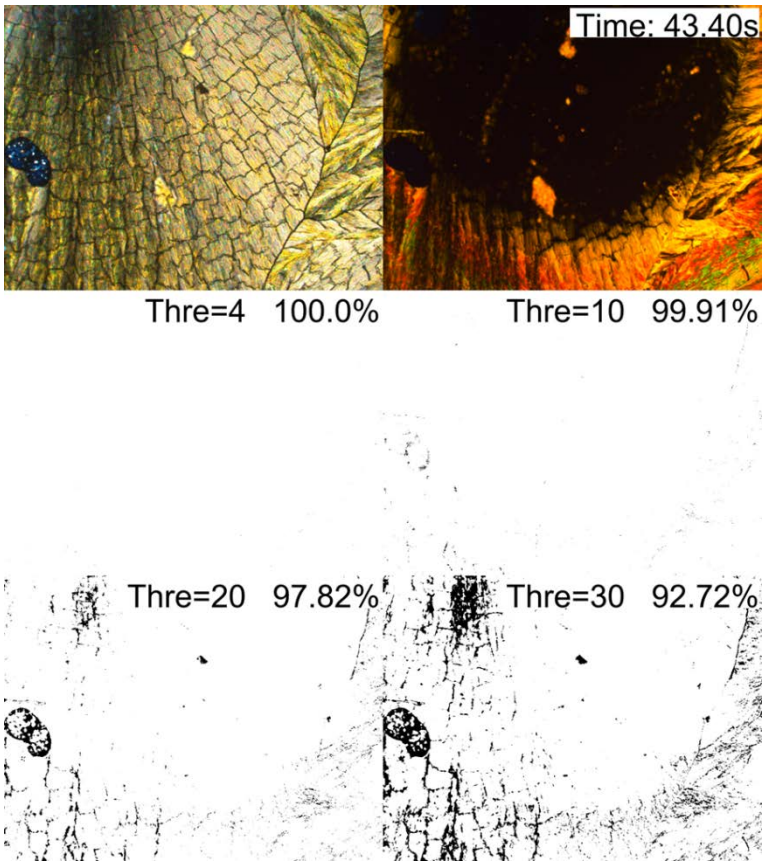

Fig. S3 Fig. S2 Demonstration of RFDA method. (a) Photos of the original condition of C1 sample; (b) Screenshot of the status when UV illumination time was 43.4 s; (c-f) Compare figure a and b pixel by pixel to calculate the difference under different thresholds.

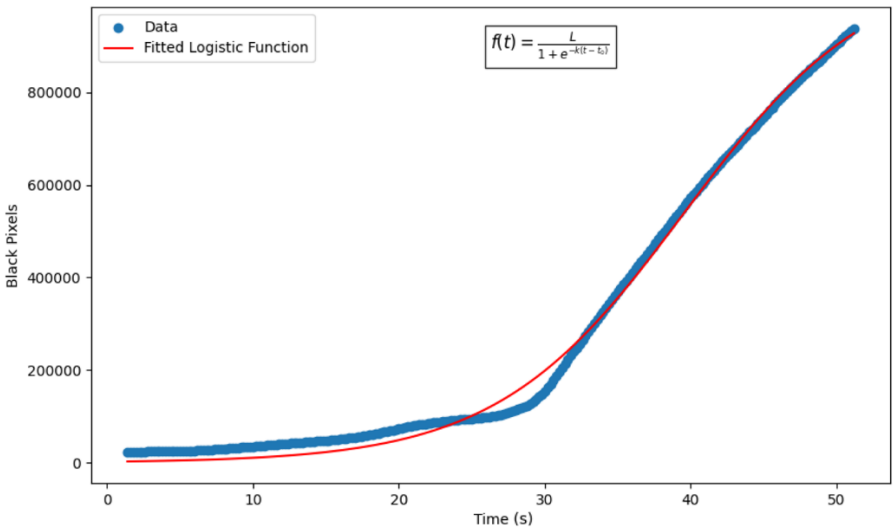

Fig. S4 The fitting results of the photoinduced solid-to-liquid phase transition process of sample sample C1 (~5 μm) with BAPS method (Params: L=1078280.324599939, k=0.15579666396440964, t_0=39.556737048544605; R_squared: 0.9951554081230224; RSS: 106983246858.81955; MSE: 427932987.4352782)

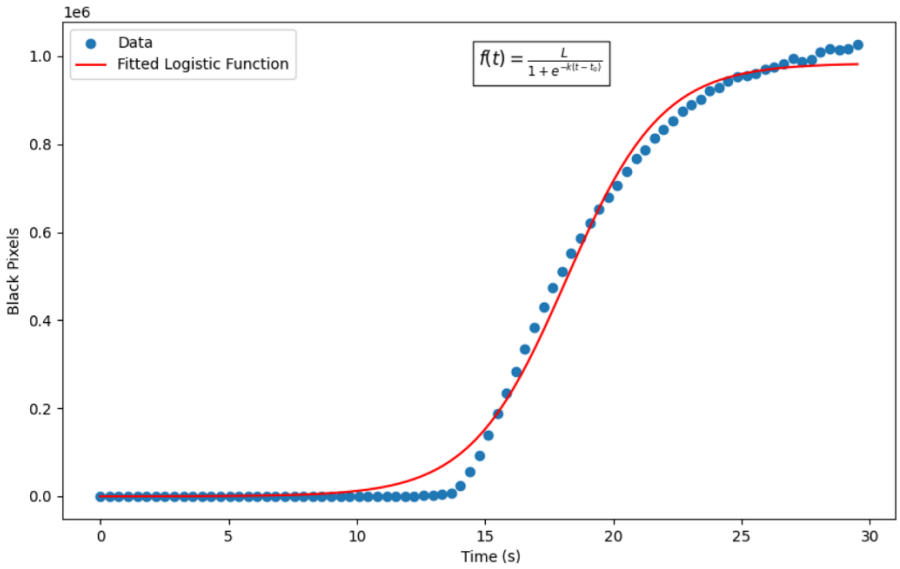

Fig. S5 The fitting results of the photoinduced solid-to-liquid phase transition process of sample C2 (~5 μm) with BAPS method (Params: L=983907.9002463985, k=0.5362605575306957, t_0=18.167349655519264; R_squared: 0.9956452097687404; RSS: 62906835628.20877; MSE: 757913682.2675755)

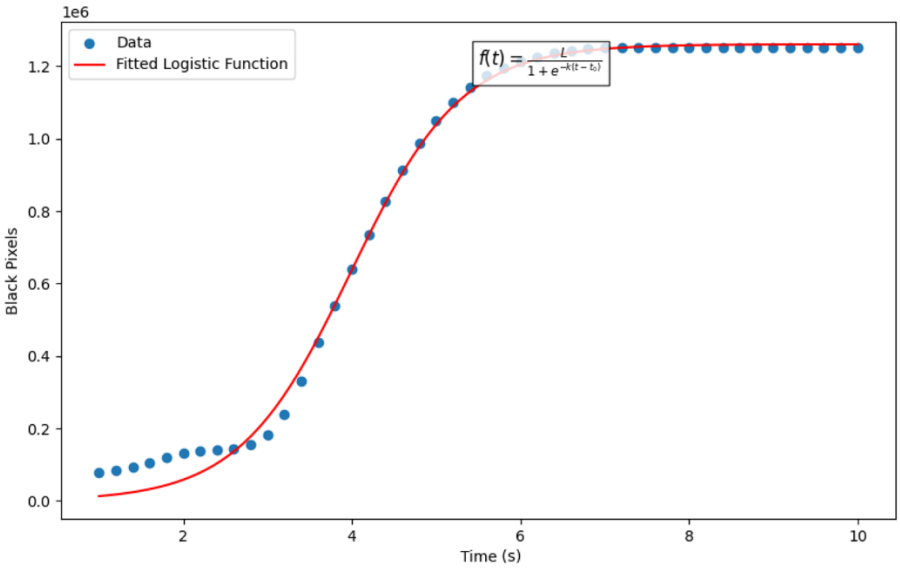

Fig. S6 The fitting results of the photoinduced solid-to-liquid phase transition process of sample C2 (~3 μm) with BAPS method (Params: L=1260429.8380949865, k=1.522408866301831, t_0=3.9853568026612662; R_squared: 0.9958390161400614; RSS: 43779283531.93706; MSE: 951723555.04211)

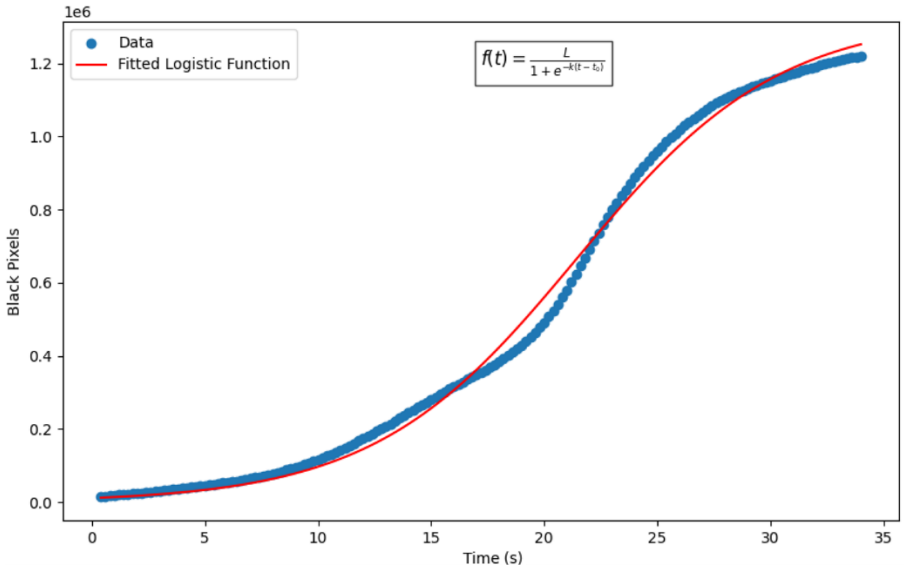

Fig. S7 The fitting results of the photoinduced solid-to-liquid phase transition process of sample C3 (~5 μm) with BAPS method (Params: L=1328121.493633524, k=0.22289647508031482, t_0=21.41315879284214; R_squared: 0.9956802114539569; RSS: 141447989279.39124; MSE: 836970350.7656286)

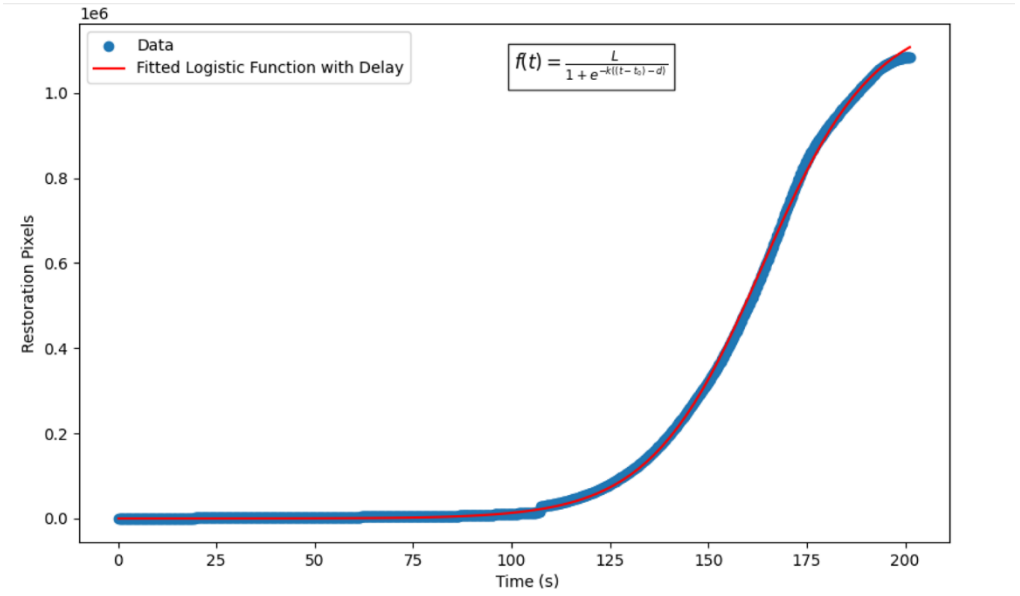

Fig. S8 The fitting results of the liquid-to-solid recovery process of sample C2 (~3 μm) with BAPS method. Different from the solid-to-liquid phase change stage, parameter d is added to indicating the delay time of the slow recovery stage (Params: L=1186849.5821699908, k=0.07030364089491738, t_0=125.93047404668755, d= 37.81221449976451; R_squared: 0.9995103120550874; RSS: 61338848531.35004; MSE: 60973010.468538806).

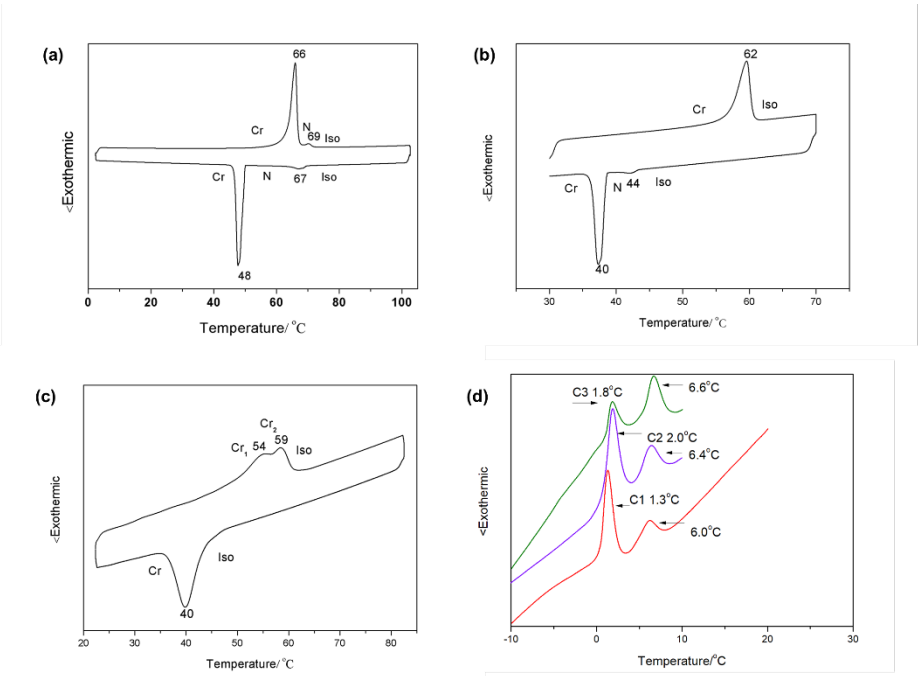

Fig. S9 Melting point results with DSC. (a) Compound C1 trans state; (b) Compound C2 trans state; (c) Compound C3 trans state. (d) C1, C2 and C3 trans/cis mixture at PSS.

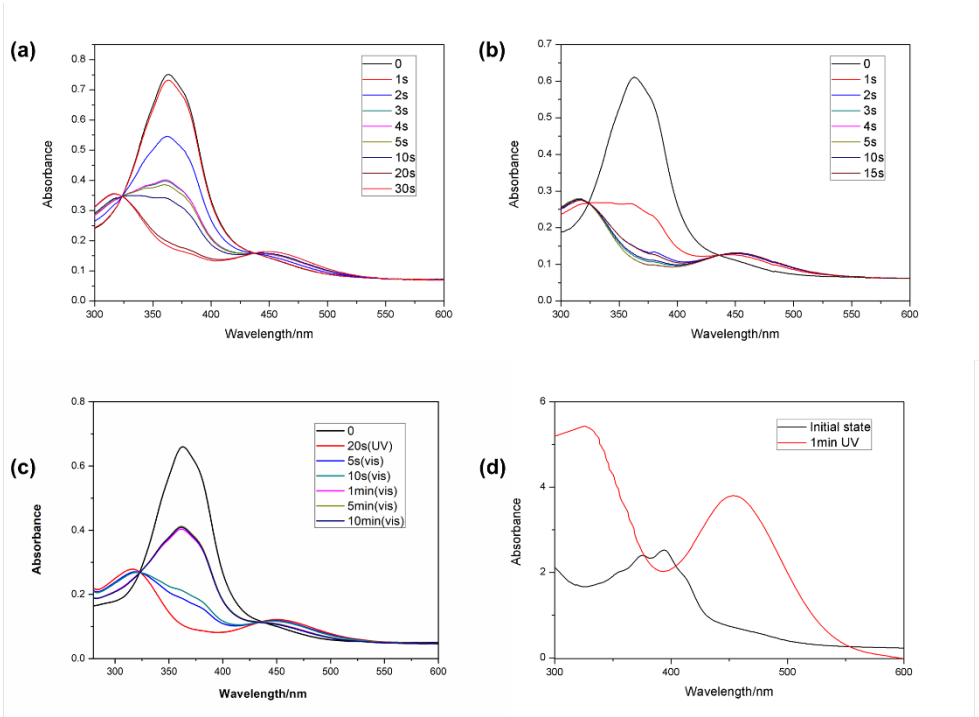

Fig. S10 UV-vis absorption spectra of compound C1. (a) Light intensity of 20 mW/cm^2 in chloroform solution; (b) Light intensity of 120 mW/cm^2 in chloroform solution; (c) UV and then visible light irradiation results in chloroform solution; (d) Spectra of film state.

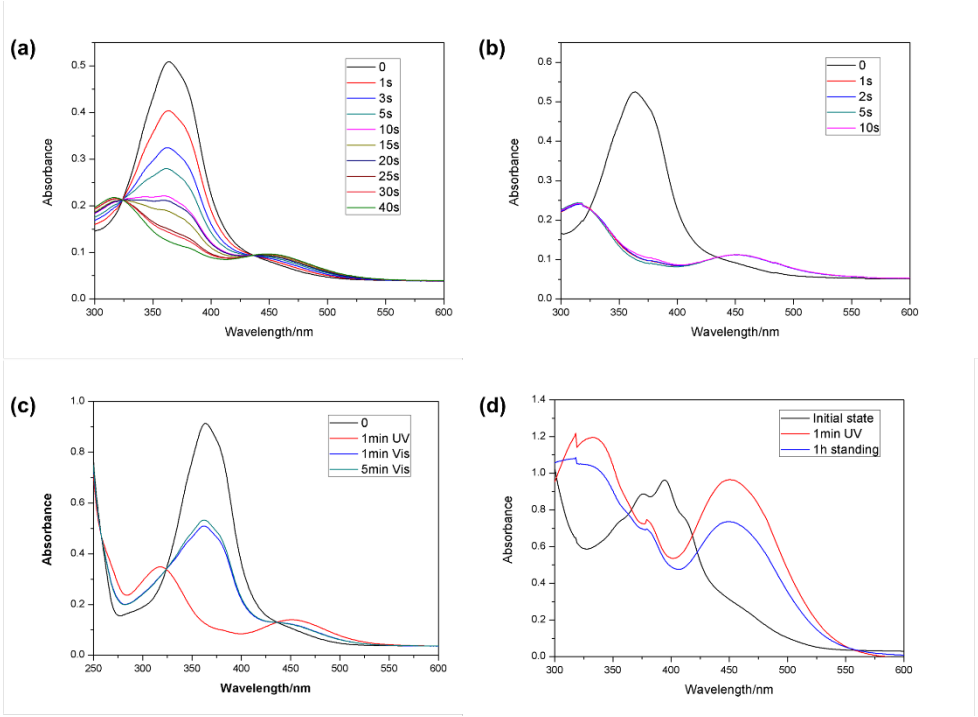

Fig. S11 UV-vis absorption spectra of compound C2. (a) Light intensity of 20 mW/cm^2 in chloroform solution; (b) Light intensity of 120 mW/cm^2 in chloroform solution; (c) UV and then visible light irradiation results in chloroform solution; (d) Spectra of film state.

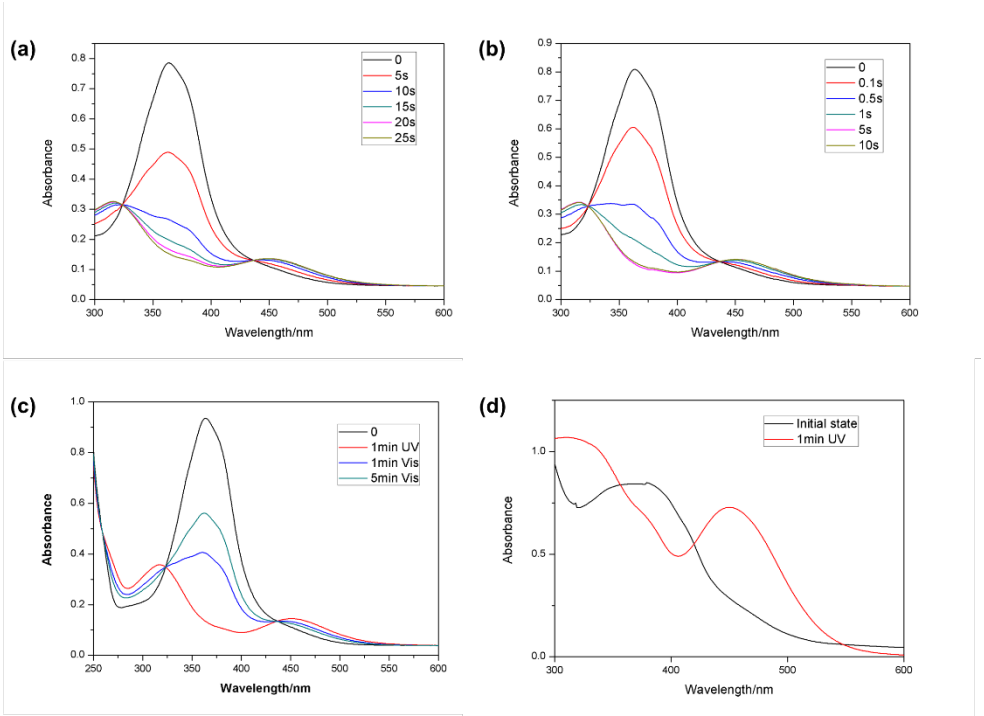

Fig. S12 UV-vis absorption spectra of compound C3. (a) Light intensity of 20 mW/cm^2 in chloroform solution; (b) Light intensity of 120 mW/cm^2 in chloroform solution; (c) UV and then visible light irradiation results in chloroform solution; (d) Spectra of film state.

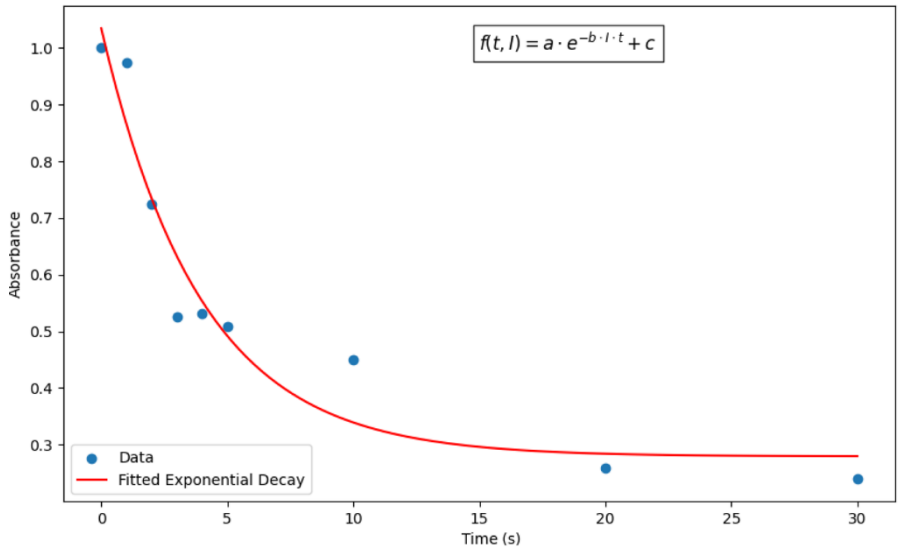

Fig. S13 Fitting results of absorption peak attenuation at UV intensity of 20 mW/cm^2 for compound C1, corresponding to Fig. S10a. (Params: a=0.7555556726958079, b=0.012668539603072092, c=0.27917511443171267; I=20; R_squared: 0.933411937639842; RSS: 0.03990126386975265; MSE: 0.00443347376330585)

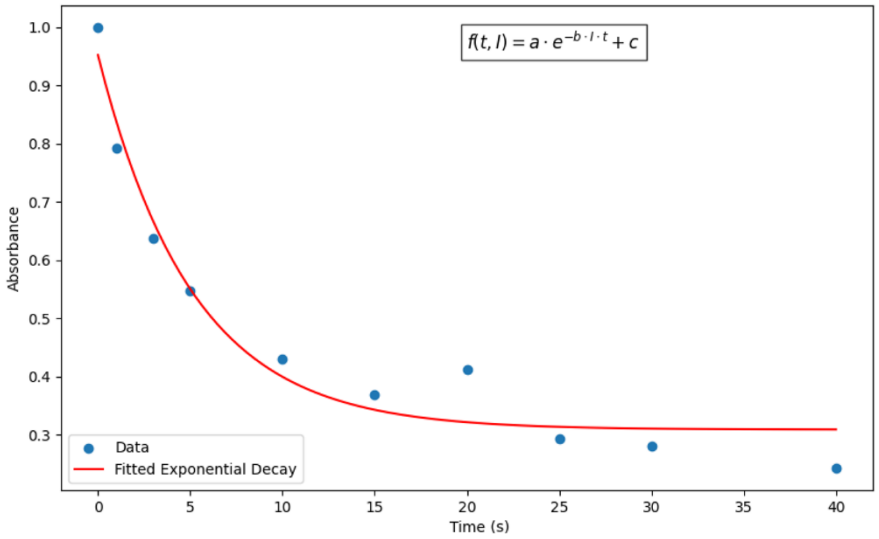

Fig. S14 Fitting results of absorption peak attenuation at UV intensity of 20 mW/cm^2 for compound C2, corresponding to Fig. S11a. (Params: a=0.6436910088048615, b=0.009790948557609017, c=0.30895518820242085; I=20; R_squared: 0.9618886266554613;RSS: 0.02071913494474867;MSE: 0.0020719134944748667)

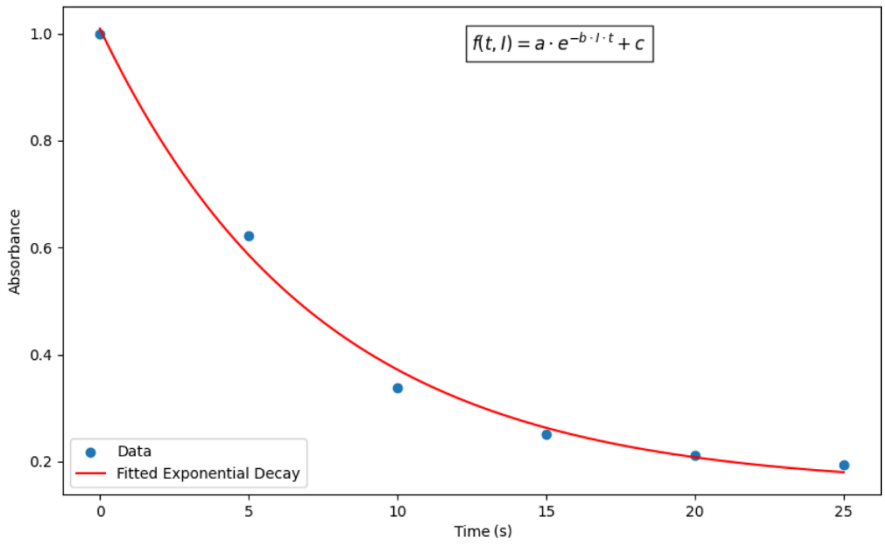

Fig. S15 Fitting results of absorption peak attenuation at UV intensity of 20 mW/cm^2 for compound C3, corresponding to Fig. S12a. (Params: a=0.8577107597178338, b=0.006791642113654158, c=0.151235645739271, I=20; R_squared: 0.9943504600684157; RSS:0.0028545278561157342;MSE: 0.0004757546426859557)

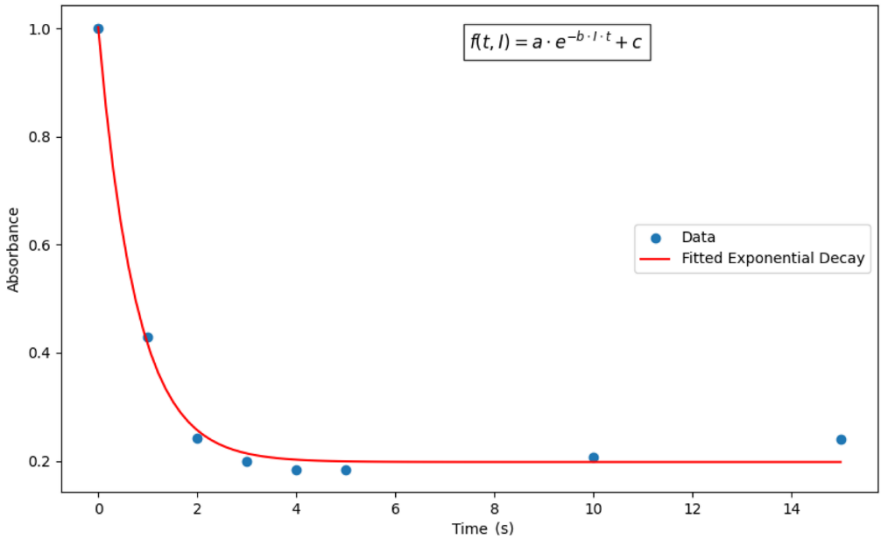

Fig. S16 Fitting results of absorption peak attenuation at UV intensity of 120 mW/cm^2 for compound C1, corresponding to Fig. S10b. (Params: a=0.8042820579689904, b=0.010896205901298495, c=0.19776672615970708; I=120; R_squared: 0.9943879975285479;RSS:0.0030820957574323035;MSE:0.0003852619696790379 4)

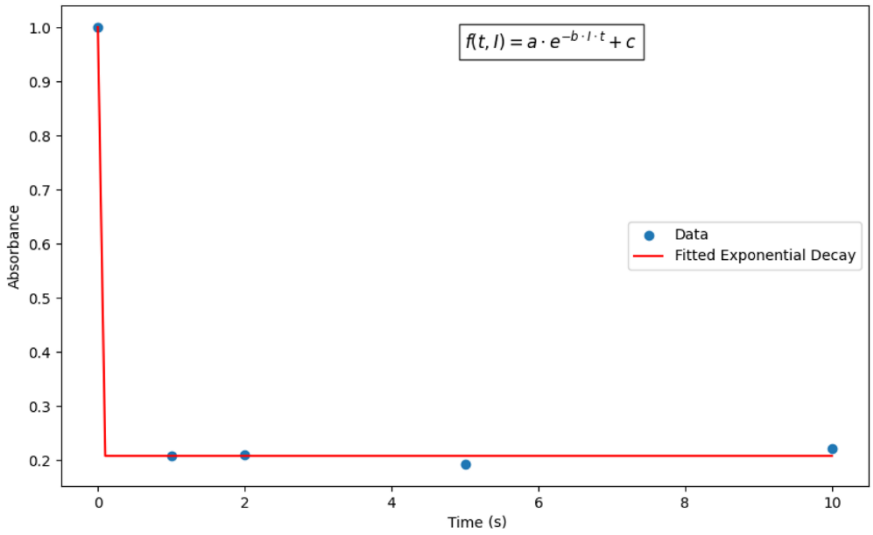

Fig. S17 Fitting results of absorption peak attenuation at UV intensity of 120 mW/cm^2 for compound C2, corresponding to Fig. S11b. (Params: a= 0.7921675000195147, b=1.1686507258057264, c=0.20783249999594133; I=120; R_squared: 0.9991720919341727;RSS: 0.0004159736749999996;MSE: 8.319473499999993e-05)

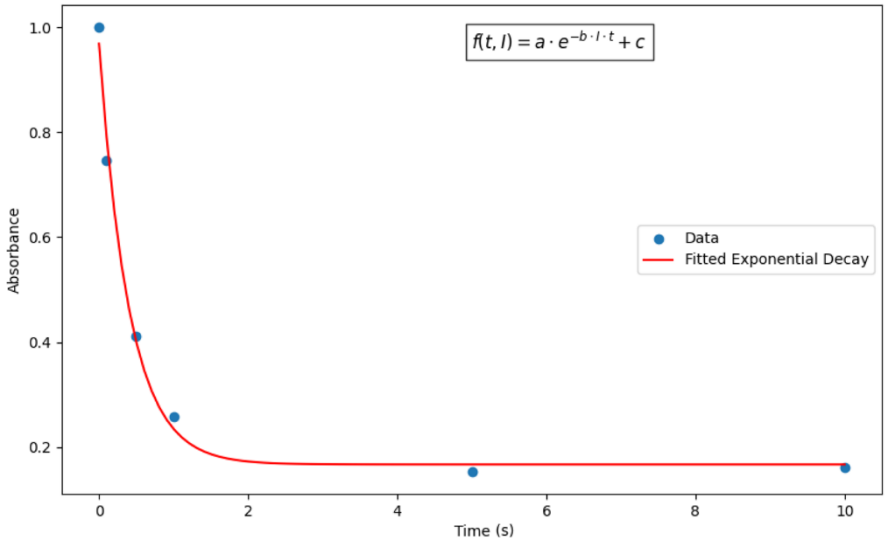

Fig. S18 Fitting results of absorption peak attenuation at UV intensity of 120 mW/cm^2 for compound C3, corresponding to Fig. S12b. (Params: a=0.8012622362846589, b=0.02057608432531268, c=0.16716856118745832, I=120; R_squared: 0.9930786803360229;RSS: 0.004147023643944279 5;MSE: 0.0006911706073240466)

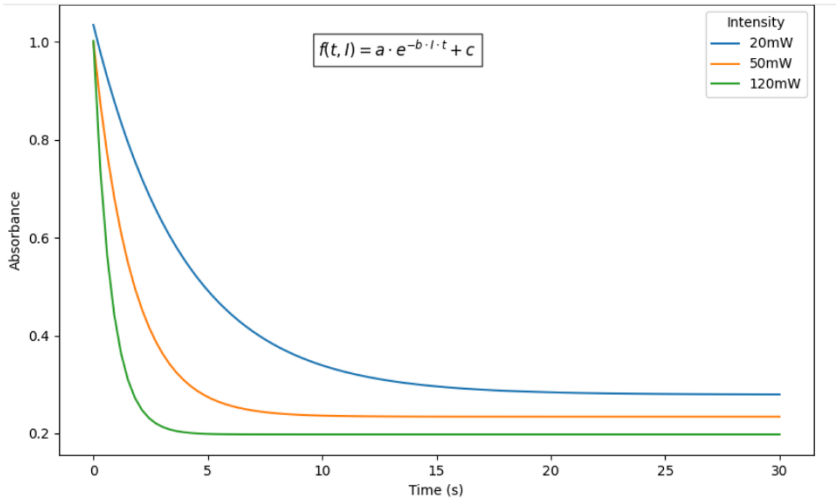

Fig. S19 Compound C1, UV intensity 50 mW/cm^2, absorption peak attenuation prediction results. (Params: a=0.7658353180078011, b=0.011782372752185329, c=0.23416468199219895, I=50)

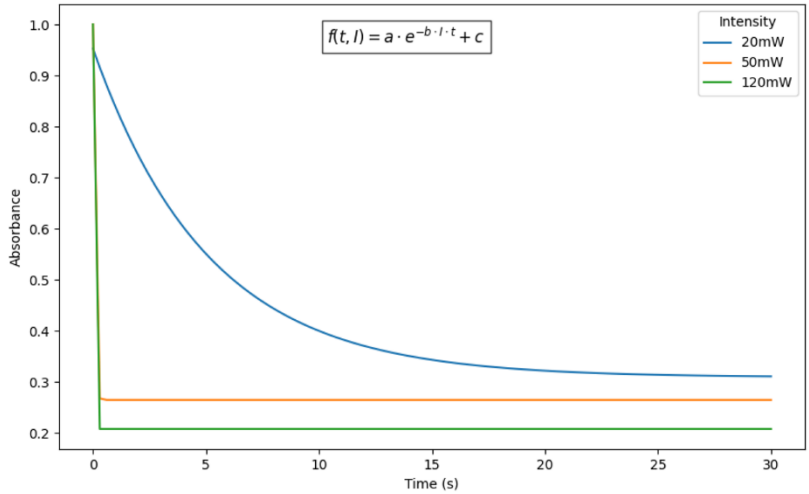

Fig. S20 Compound C2, UV intensity 50 mW/cm^2, absorption peak attenuation prediction results. (Params: a=0.7353398229611056, b=0.3679189320770872, c=0.2646601770388946, I=50)

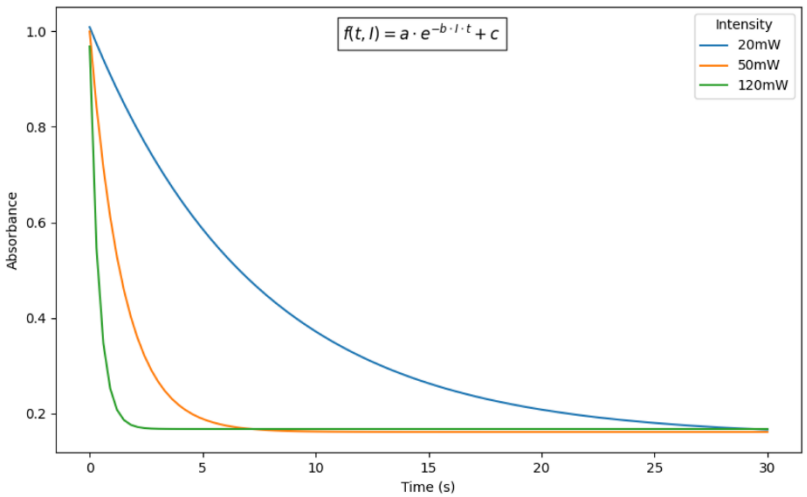

Fig. S21 Compound C3, UV intensity 50 mW/cm^2, absorption peak attenuation prediction results. (Params: a=0.8389764955036513, b=0.013683863219480829, c=0.161023504496295, I=50)

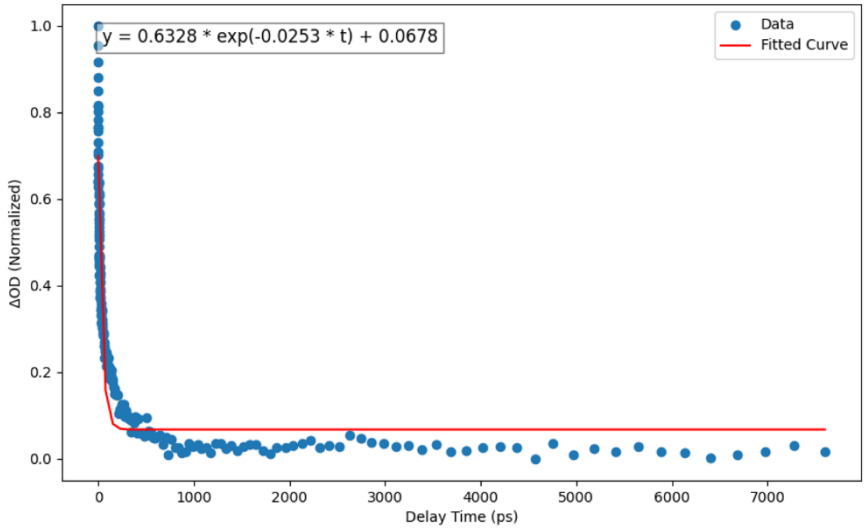

Fig. S22 TAS attenuation fitting results for C1, corresponding to Fig. 6c. (Half-life: 27.349283; R-squared: 0.925216; Residual Sum of Squares (RSS): 0.924661; Mean Squared Error (MSE): 0.004718)

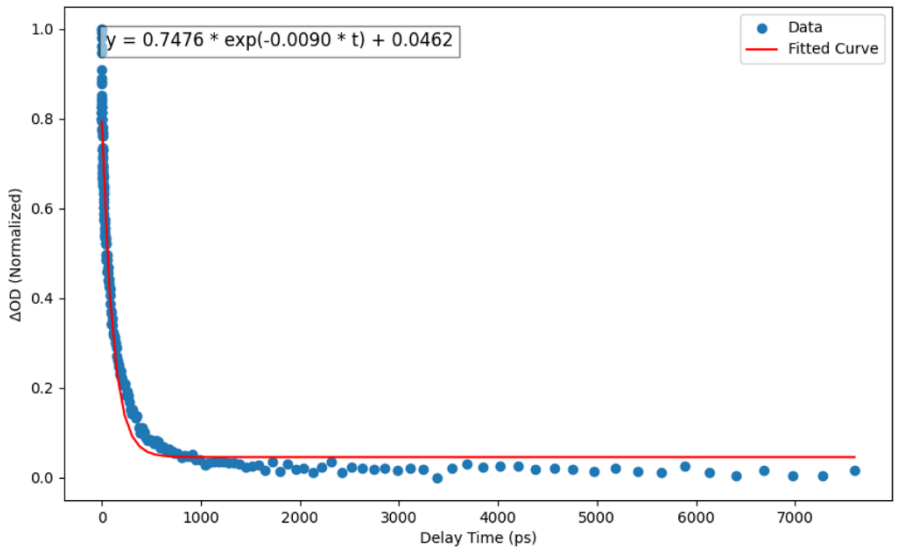

Fig. S23 TAS attenuation fitting results for C2, corresponding to Fig. 6c. (Half-life: 76.622619; R-squared: 0.972490; Residual Sum of Squares (RSS): 0.551172; Mean Squared Error (MSE): 0.002715)

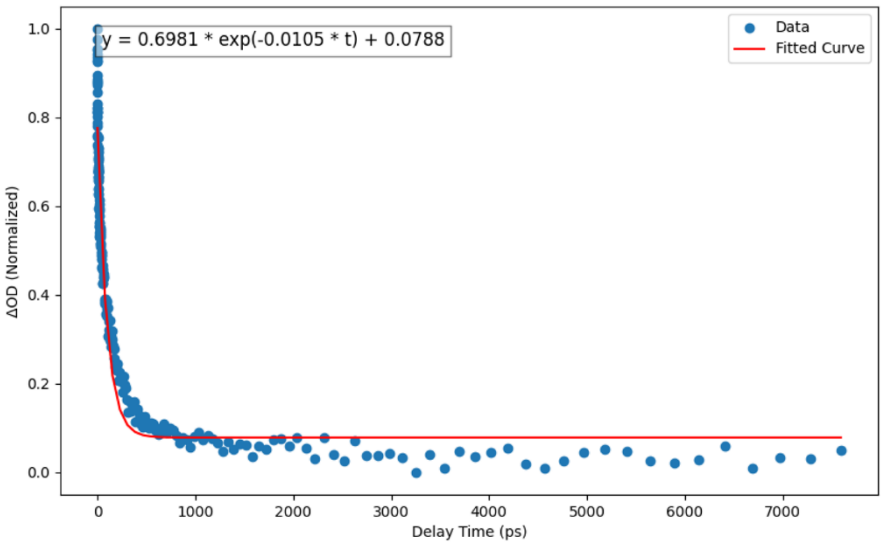

Fig. S24 TAS attenuation fitting results for C3, corresponding to Fig. 6c. (Half-life: 65.975082; R-squared: 0.955344; Residual Sum of Squares (RSS): 0.780887; Mean Squared Error (MSE): 0.003866)

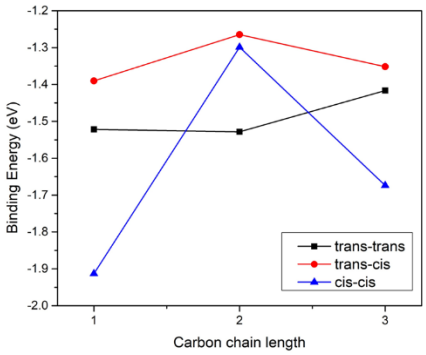

Fig. S25 The Simulated results of the isomer combinations' intermolecular interaction energy.

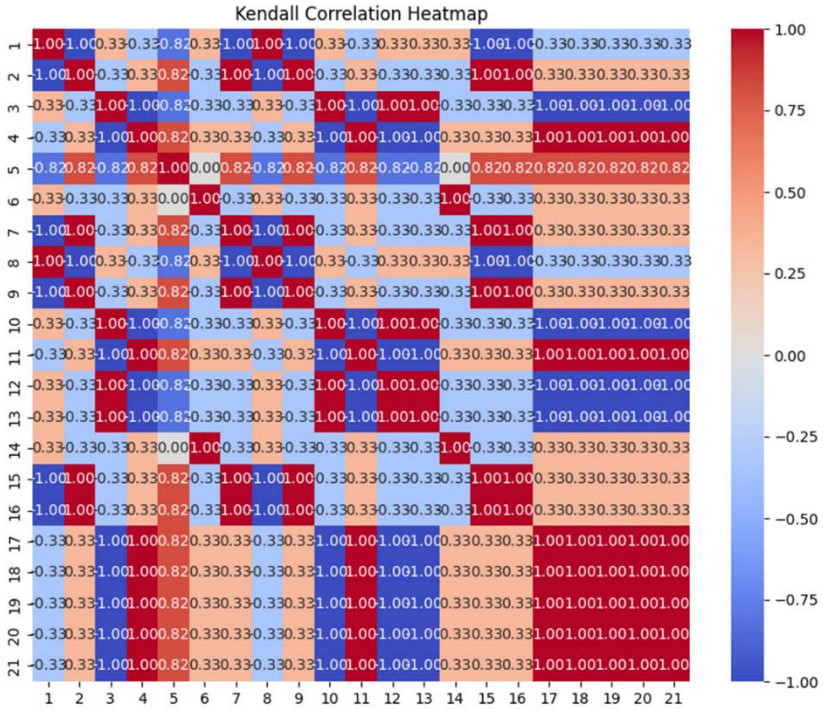

Fig. S26 Kendall's tau coefficient was used to evaluate the correlation of performance parameters, corresponding to Table 1.

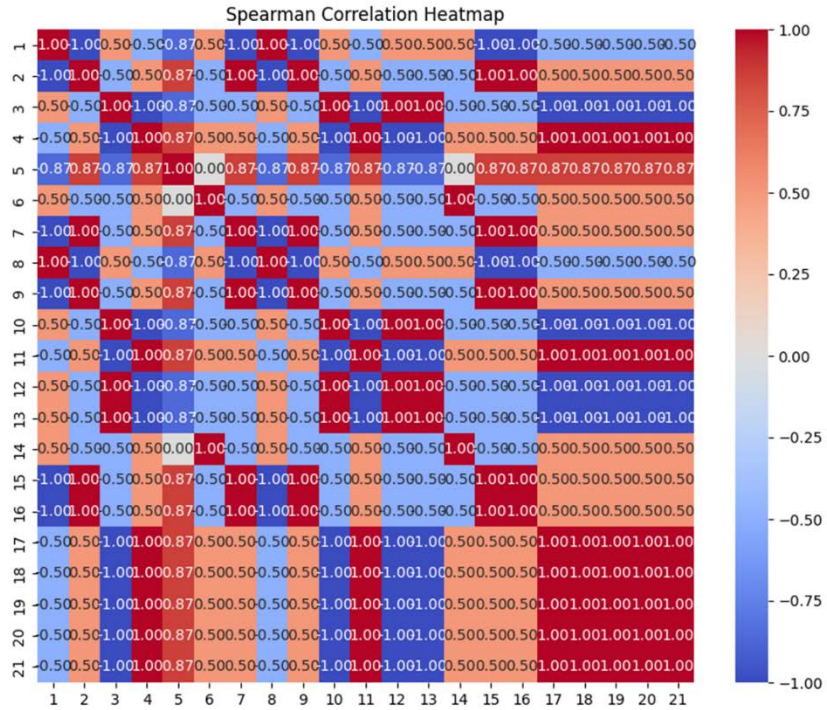

Fig. S27 Spearman's rank correlation coefficient was used to evaluate the correlation of performance parameters, corresponding to Table 1.

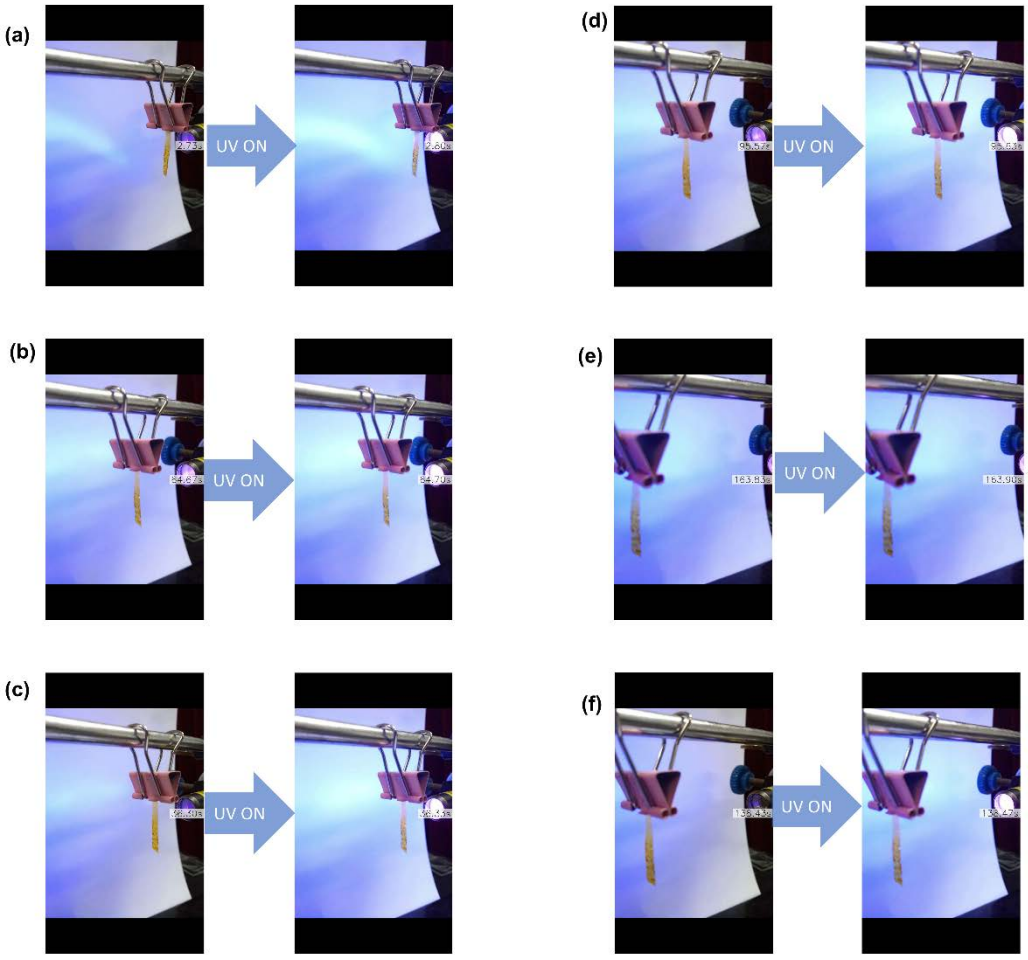

Fig. S28 The deformation start-up time of C2-based composite film photo-actuator after UV light was turned on. (a) 1 cm illumination distance: 0.07 s; (b) Illumination distance of 2 cm: 0.03 s; (c) Light distance of 3 cm: 0.03 s; (d) Light distance of 4 cm: 0.06 s; (e) Light distance of 5 cm: 0.07 s; (f) Light distance of 6 cm: 0.04 s; No significant correlation between light intensity and start-up time was observed.

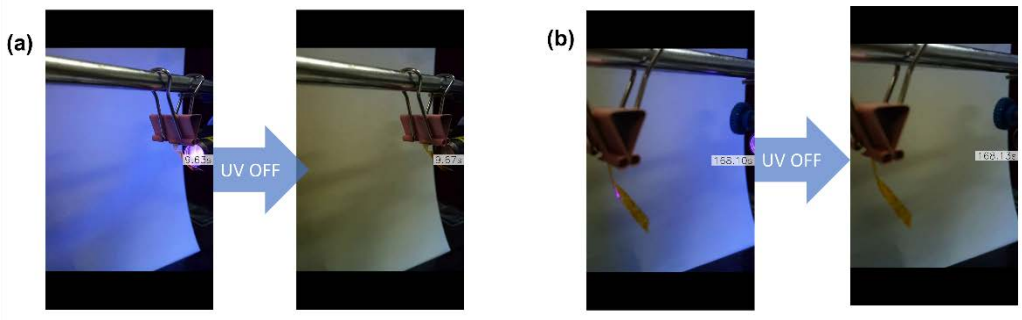

Fig. S29 The recovery stage start-up time of C2-based composite film photo-actuator after UV light was turned off. (a) Light distance of 1cm: 0.04 s; (b) Light distance of 6cm: 0.03 s; There was no significant correlation between light intensity and start-up time.

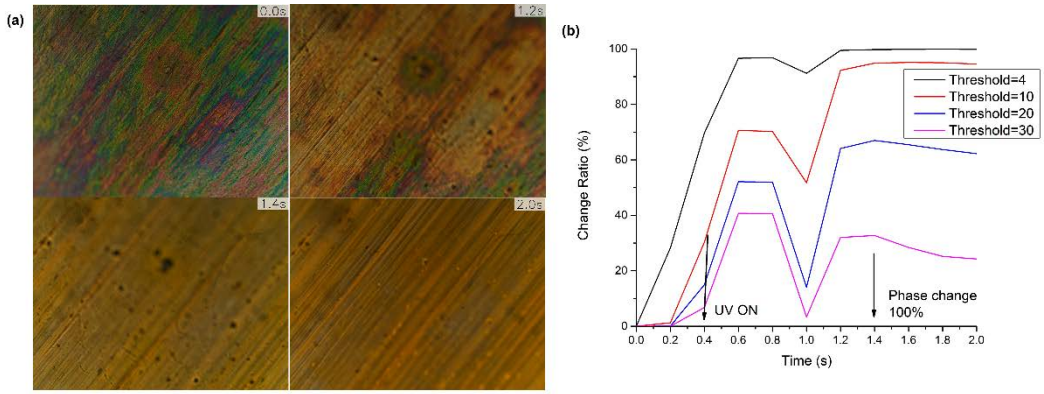

Fig. S30 POM was used to observe the phase transition behavior of C1-based composite film after UV light was turned on (Supplementary Video 3). (a) Video frames; (b) The start-up time of phase transition was determined by RFDA method.

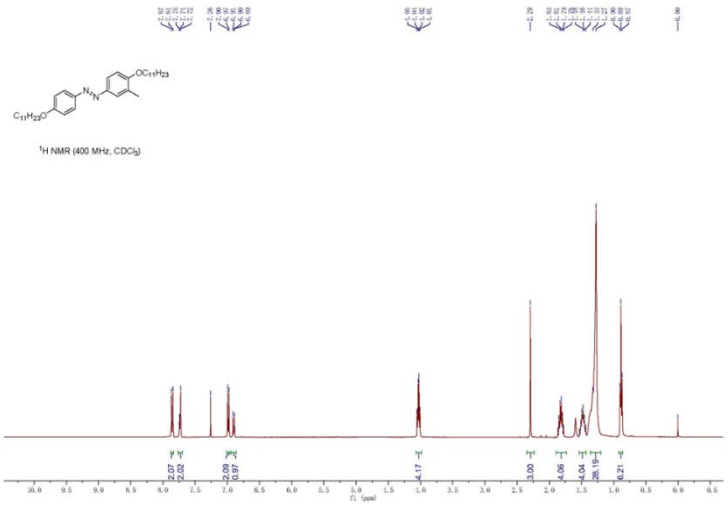

Fig. S31 ^{1}H NMR of compound C1.

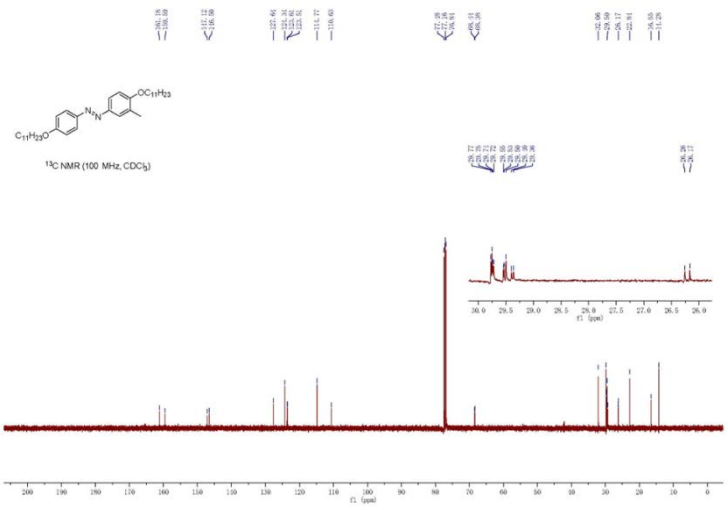

Fig. S32 ^{13}C NMR of compound C1.

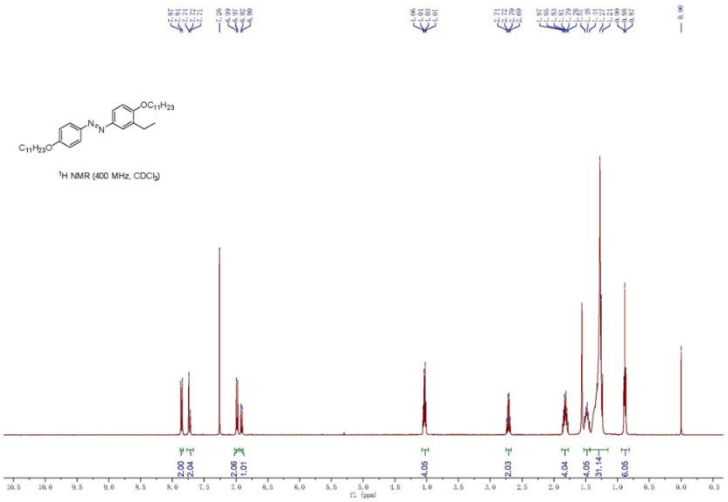

Fig. S33 ^{1}H NMR of compound C2.

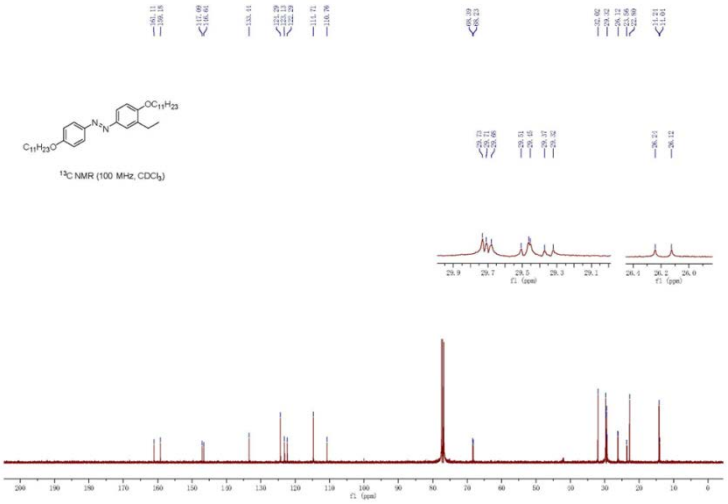

Fig. S34 ^{13}C NMR of compound C2.

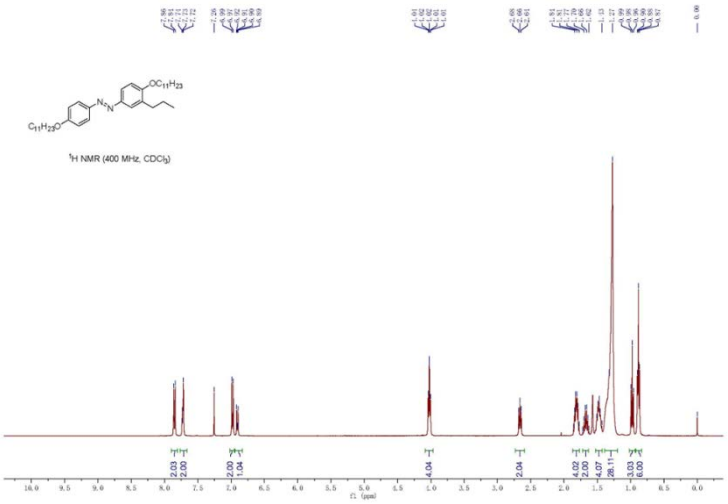

Fig. S35 ^{1}H NMR of compound C3.

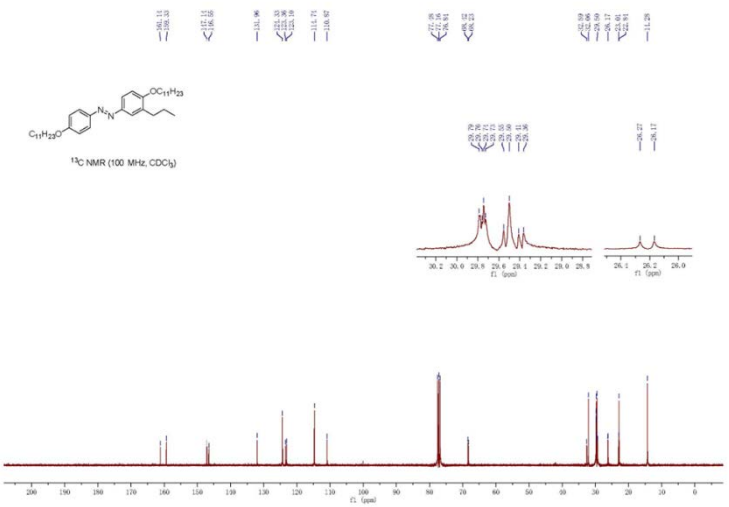

Fig. S36 ^{13}C NMR of compound C3.

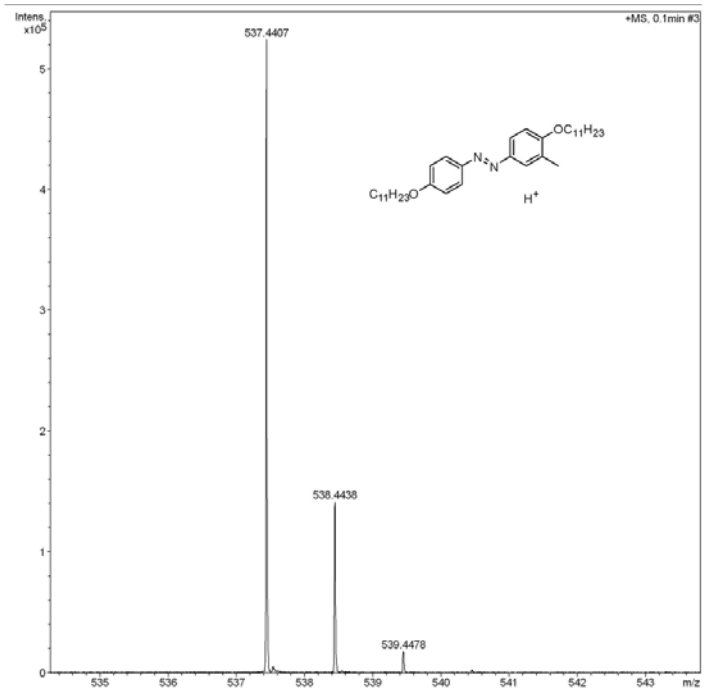

Fig. S37 Mass spectrum of compound C1.

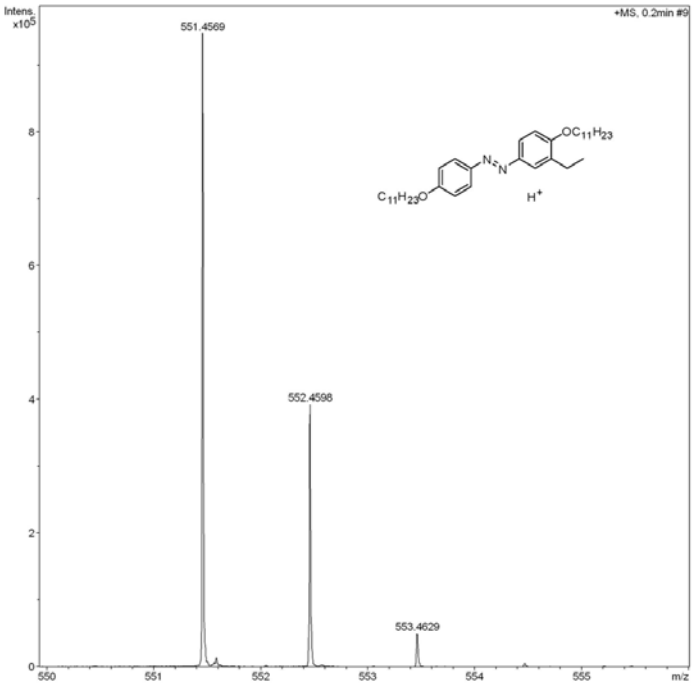

Fig. S38 Mass spectrum of compound C2.

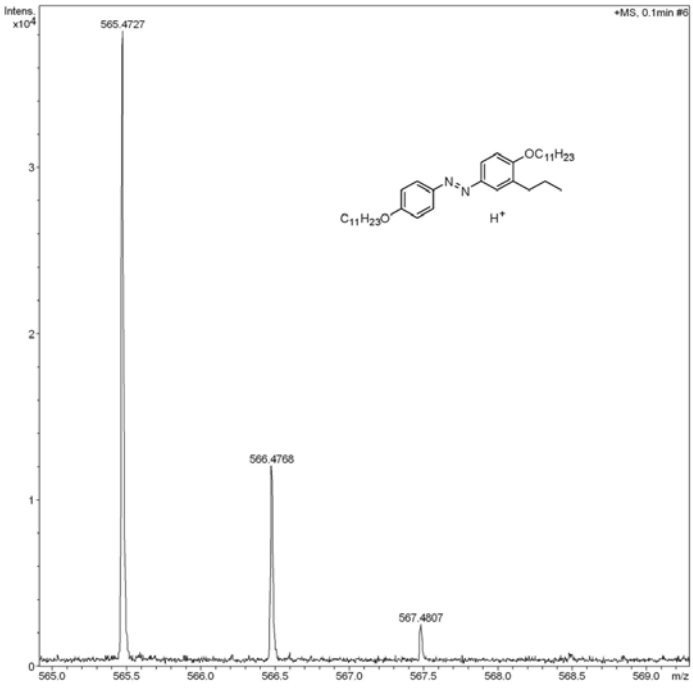

Fig. S39 Mass spectrum of compound C3.

2. Supplementary Video

Video S1. Photoinduced solid-to-liquid phase transition of pure compound observed in-situ by POM. (1) C1; (2) C2; (3) C3.

Video S2. Deformation of the composite film optical actuators. (1) C1 strip sample; (2) C2 strip sample; (3) C2 large block sample; (4) C3 large block sample.

Video S3. Photoinduced solid-to-liquid phase transition of C1 composite film observed in-situ by POM.